A ruthenium-titania core–shell nanocluster catalyst for efficient and durable alkaline hydrogen evolution

Hyun Woo Lim,[a] Tae Kyung Lee,[bc] Subin Park,[b] Dwi Sakti Aldianto Pratama,[d] Bingyi Yan,*[ae] Sung Jong Yoo,*[b] Chan Woo Lee,*[d] Jin young Kim*[af]

a. Department of Materials Science and Engineering, Seoul National University, Seoul 08826, Republic of Korea

b. Hydrogen·Fuel Cell Research Center, Korea Institute of Science and Technology (KIST), Seoul 02792, Republic of Korea

c. Department of Chemical and Biological Engineering, Korea University, Seoul 02841, Republic of Korea

d. Department of Chemistry, Kookmin University, Seoul 02707, Republic of Korea

e. School of Chemistry and Chemical Engineering, Yangzhou University, Yangzhou, Jiangsu, 225009, P. R. China

f. Research Institution of Advanced Materials (RIAM) and Institution of Engineering Research, College of Engineering, Seoul National University, Seoul 08826, Republic of Korea

*Corresponding author: Bingyi Yan; Email: bingyiyan@yzu.edu.cn

*Corresponding author: Sung Jong Yoo; Email: ysj@kist.re.kr

*Corresponding author: Chan Woo Lee; Email: cwlee1@kookmin.ac.kr

*Corresponding author: Jin Young Kim; Email: jykim.mse@snu.ac.kr

Table of Contents

Supplementary Figures

Supplementary Tables

Supplementary Figures

Figure S1. LSV curves of core–shell Ru catalysts measured at a scan rate of 10 mV s^{-1} in 1.0 M KOH electrolyte (pH = 14). As the cycle progresses, the color of the lines was expressed with lighter color.
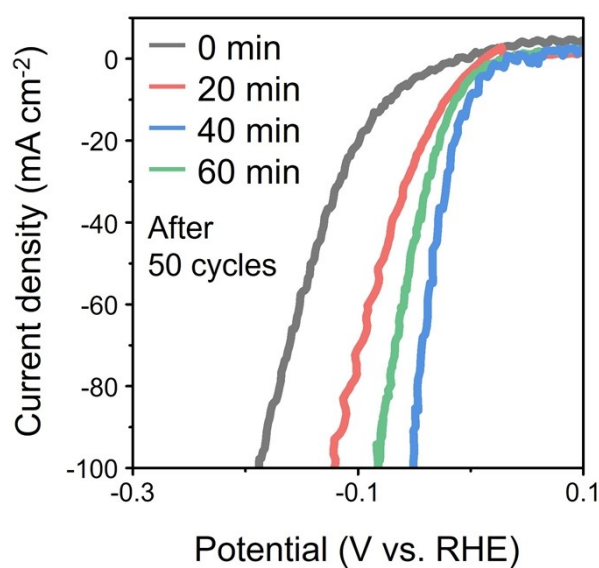
Figure S2. Magnified view of LSV curves of core–shell Ru catalysts measured at a scan rate of 10 mV s^{-1} in 1.0 M KOH electrolyte (pH = 14).
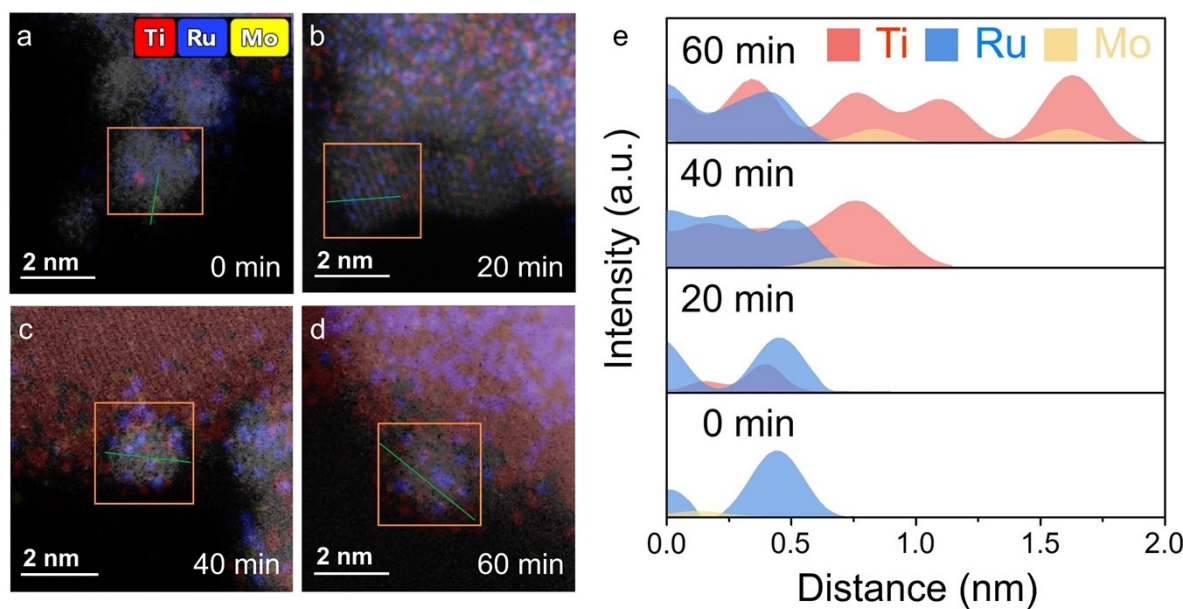
Figure S3. Elemental mapping images of (a) CS-Ru-0, (b) CS-Ru-20, (c) CS-Ru-40, and (d) CS-Ru-60 obtained through Cs-corrected HAADF-STEM EDS analysis. The images were obtained from samples before HER measurements. The orange square represents the active sites of each core–shell Ru catalyst. (e) Line-scan profiles of core–shell Ru NCs. Line-scan profiles obtained from the center to the surface of the nanocluster.
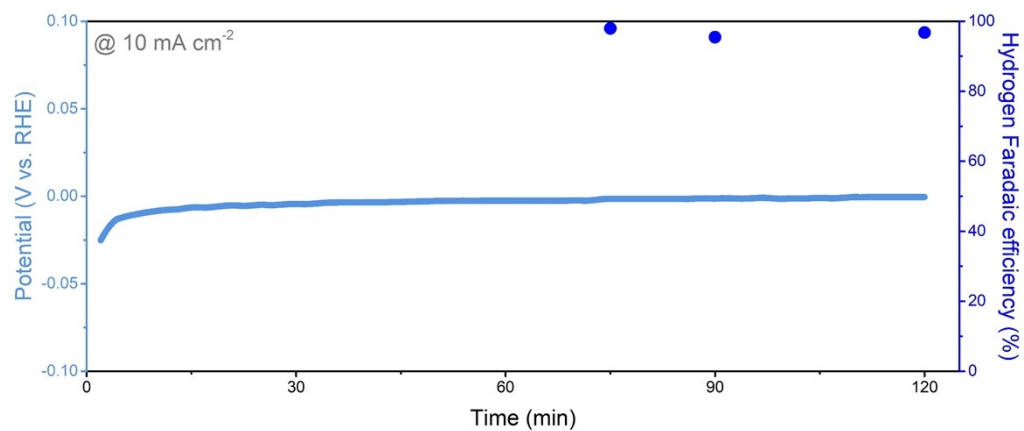
Figure S4. Faraday efficiency for H_2 production measured at the current density of 10 mA cm^{-2} using CS-Ru-40 catalyst.
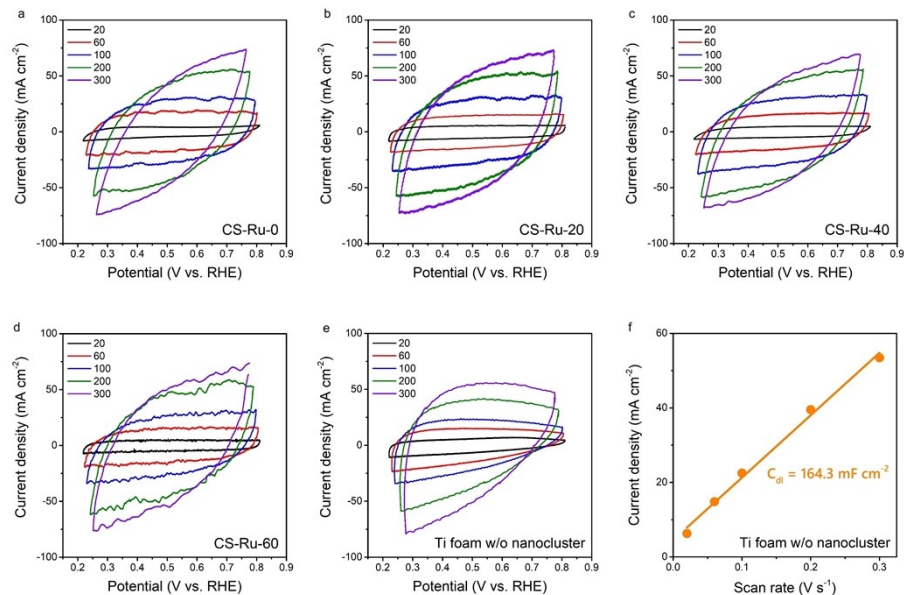
Figure S5. Cyclic voltametric scans of (a) CS-Ru-0, (b) CS-Ru-20, (c) CS-Ru-40, (d) CS-Ru-60, and (e) Ti foam without nanocluster measured in 1.0 M Na_2SO_4 (pH = 7) at numerous scan rates. The double-layer capacitance value of (f) Ti foam without nanocluster.
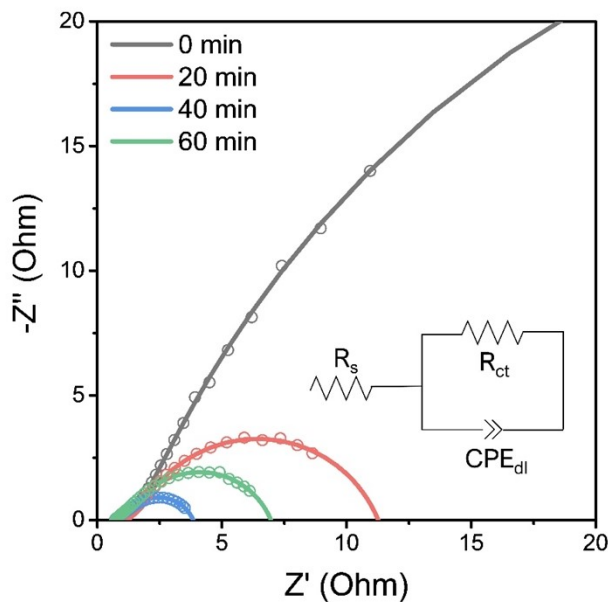
Figure S6. Nyquist plots of the fitting results for the core–shell Ru catalysts. EIS analysis was performed at an equilibrium potential of 0 V vs. RHE in 1.0 M KOH (pH = 14). The equivalent circuit model applied to simulate the EIS results is shown in the inset.
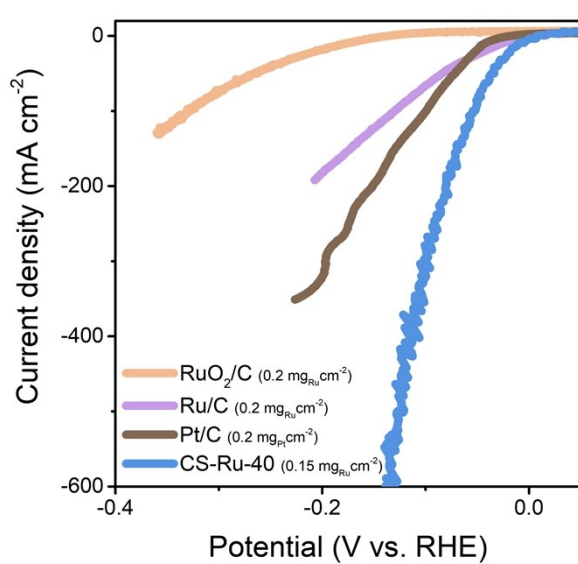
Figure S7. LSV curves of Pt/C, Ru/C, RuO$_2$/C, and CS-Ru-40 measured at a scan rate of 10 mV s^{-1} in 1.0 M KOH electrolyte (pH = 14).
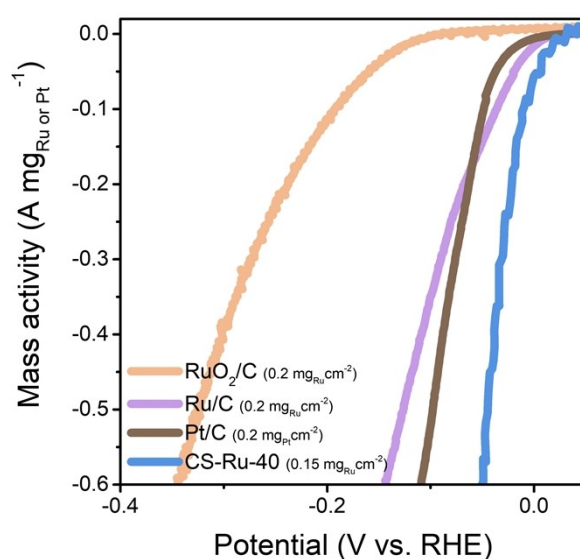
Figure S8. LSV curves of core–shell Ru, Pt/C, Ru/C, and RuO$_2$/C catalysts. The current is normalized by precious metal content.
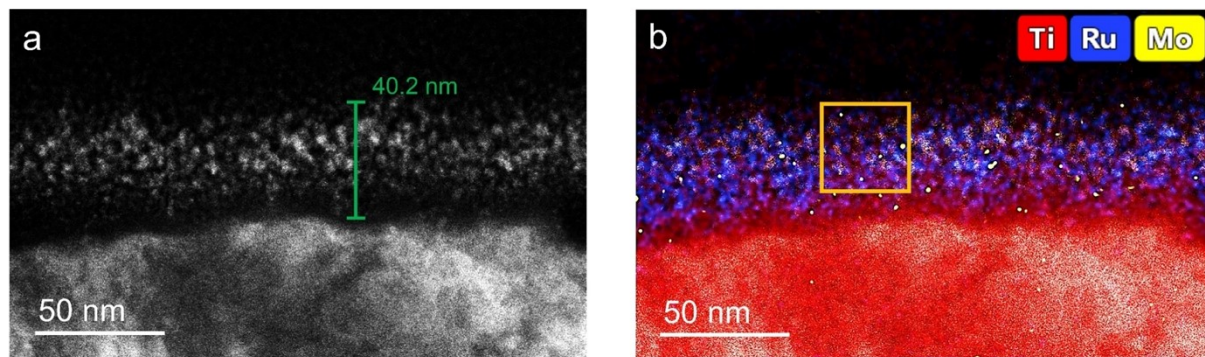
Figure S9. (a) Cross-sectional HAADF-STEM image and (b) EDS mapping image of CS-Ru-40. The image shows that the thickness of the mixed metal oxide layer is 40.2 nm.
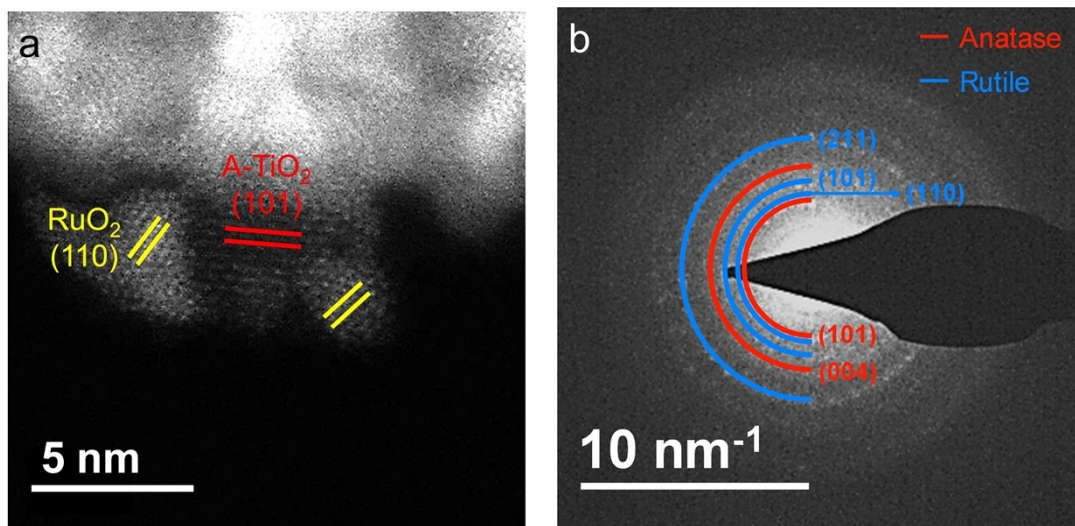
Figure S10. (a) HAADF-STEM image and (b) SAED pattern of CS-Ru-40 before HER measurements. Only anatase (red) and rutile (blue) phases are detected.
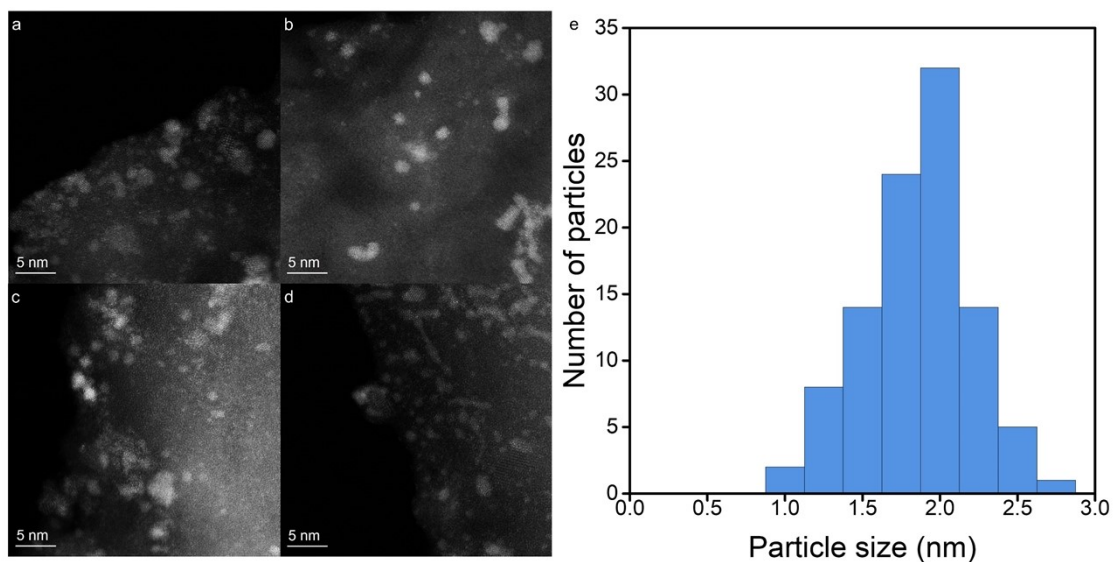
Figure S11, (a) – (d) HAADF-STEM images and (e) particle size distribution of CS-Ru-40 NCs.
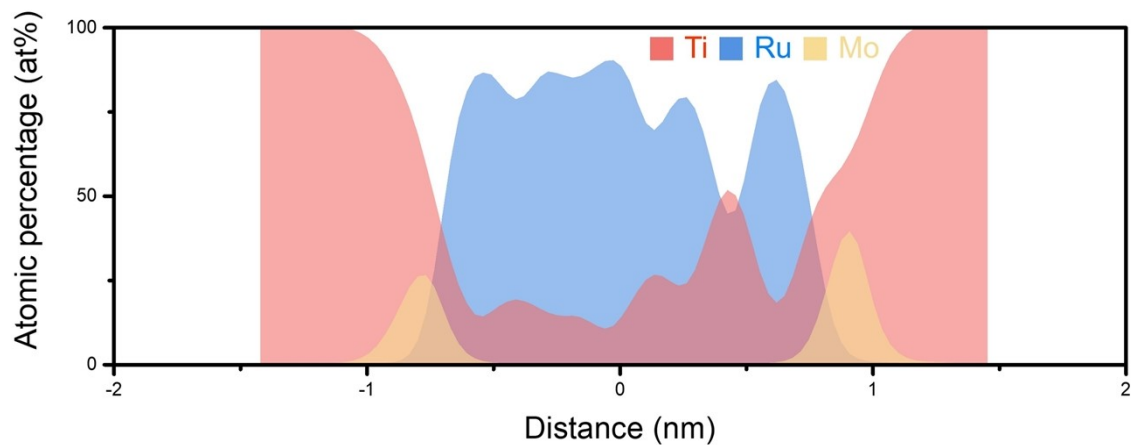
Figure S12. Line-scan profile of CS-RS-40 calculated based on the atomic percentages. Line-scan profile is obtained before HER measurement.
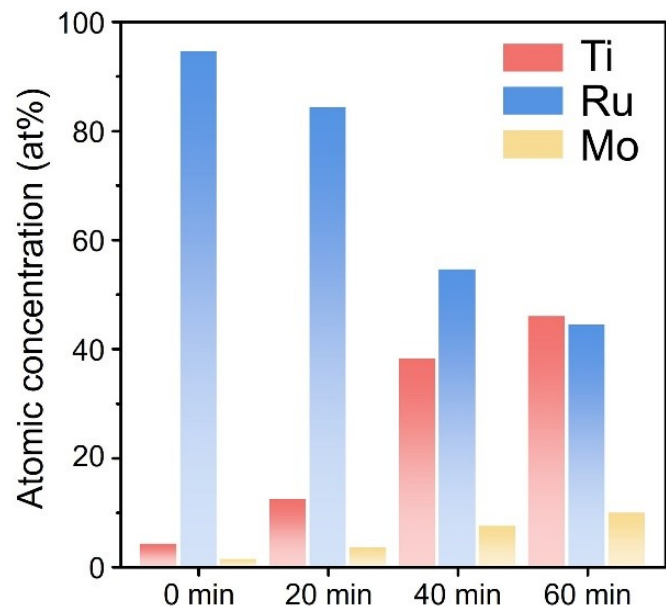
Figure S13. The atomic ratio of the core–shell Ru NC measured by elemental mapping analysis after different durations of annealing. The mapping result is obtained from one nanocluster as indicated by the orange box of Fig. S3. The data were obtained from samples before HER measurements.
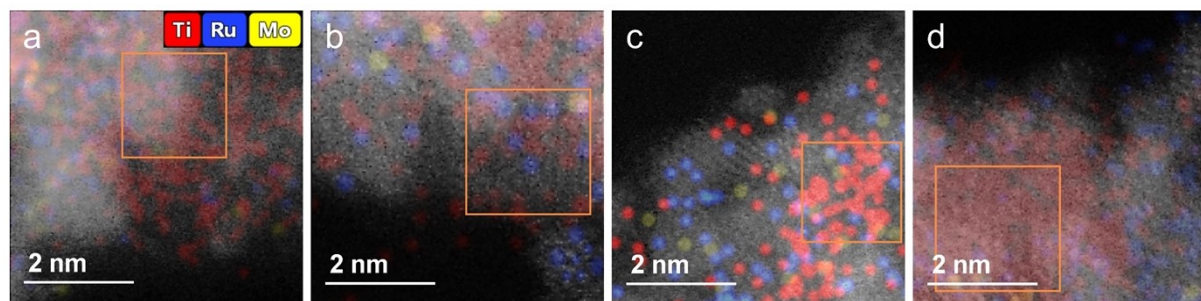
Figure S14. Elemental mapping images of (a) CS-Ru-0, (b) CS-Ru-20, (c) CS-Ru-40, and (d) CS-Ru-60 obtained through Cs-corrected HAADF-STEM EDS analysis. The images were obtained from samples before HER measurements. The orange square represents the supports of each core–shell Ru catalyst.
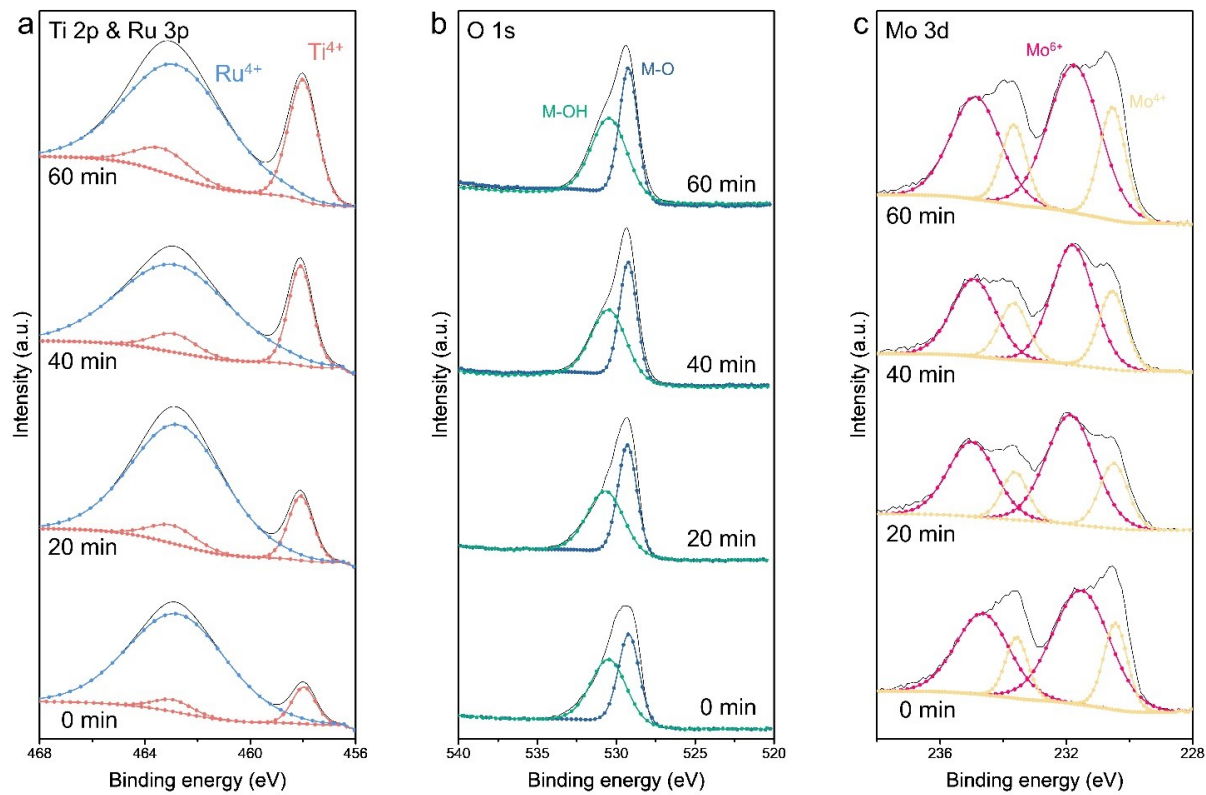
Figure S15. XPS core-level spectra of the (a) Ti 2p and Ru 3p, (b) O 1s, and (c) Mo 3d region for core–shell Ru catalysts before HER measurements.
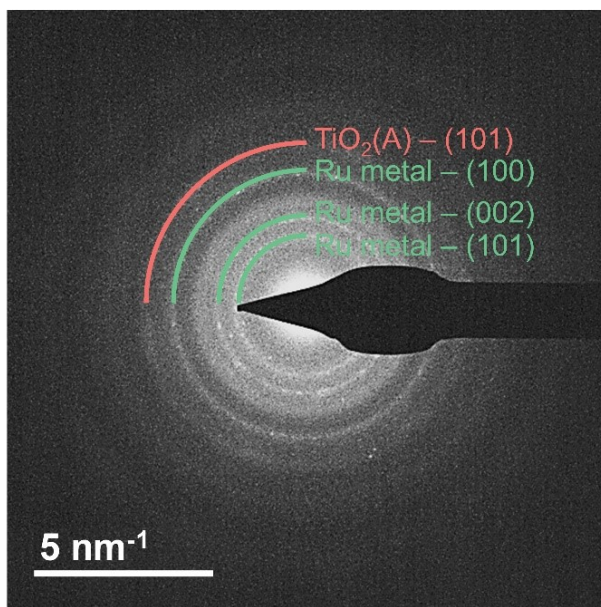
Figure S16. SAED pattern of CS-Ru-40. Only anatase (red) and Ru metal (green) phases are detected.
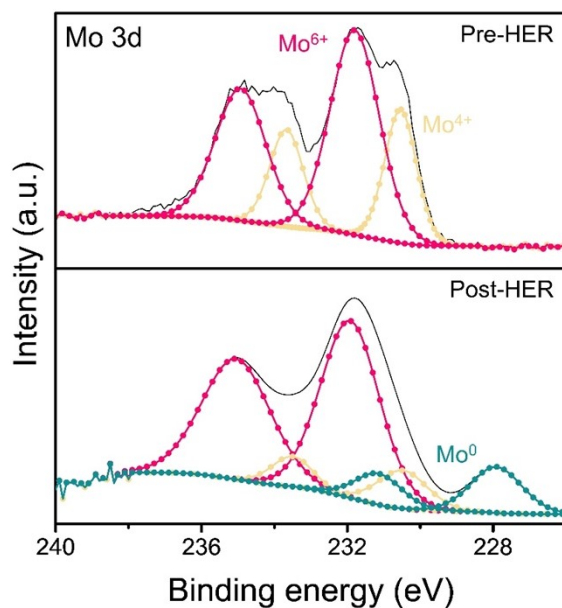
Figure S17. XPS core-level spectra of the Mo 3d for core–shell Ru catalyst according to the HER measurements.
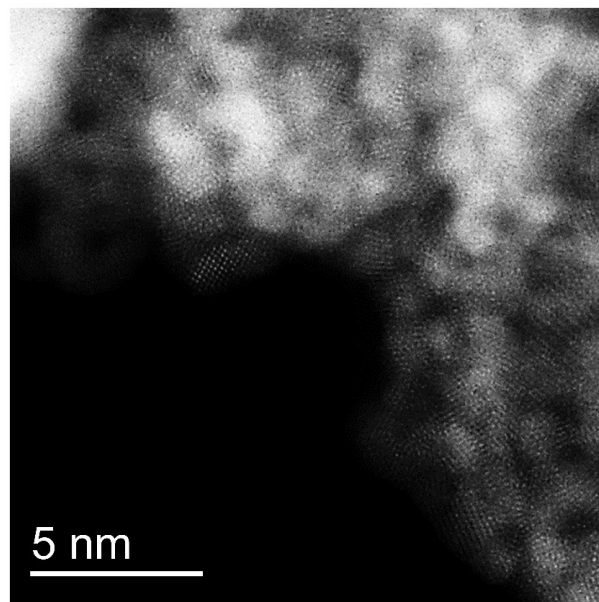
Figure S18. Enlarged view of HAADF-STEM image of CS-Ru-40.
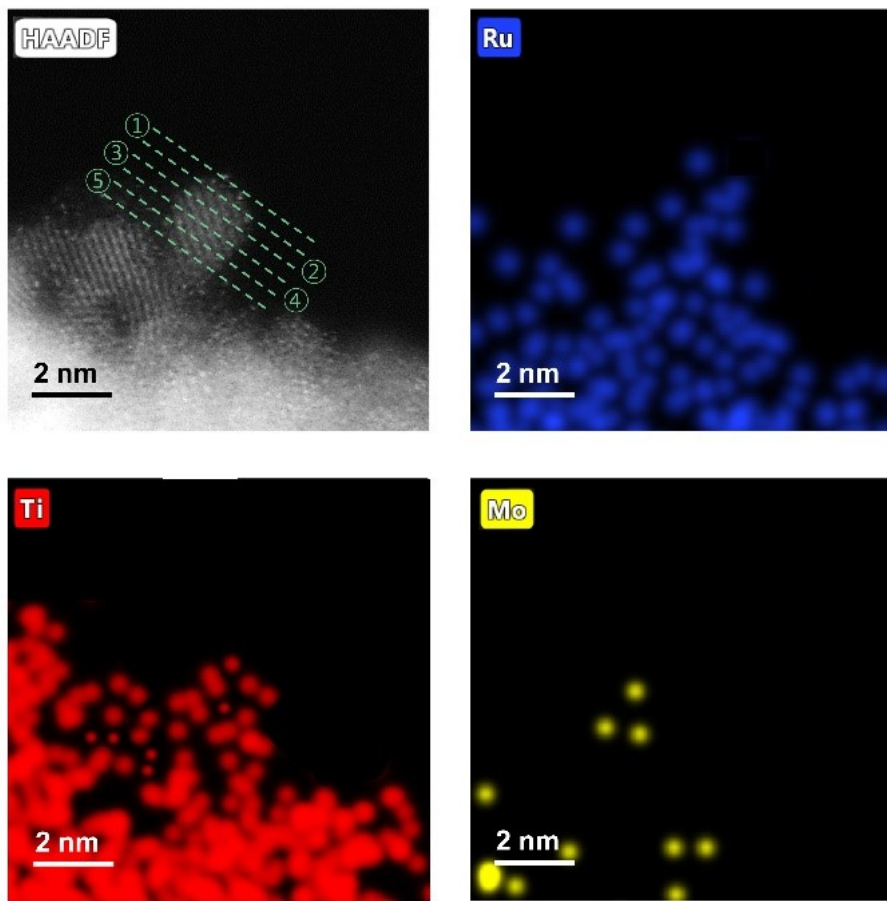
Figure S19. Elemental mapping images of CS-Ru-40. Spherical CS-Ru-40 nanocluster was divided into five sections and quantitatively analyzed by EDS line-scan analysis.
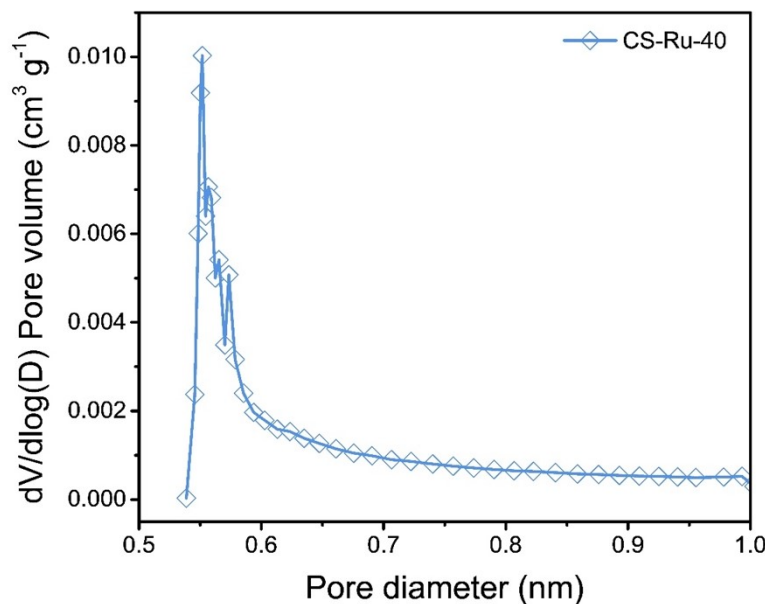
Figure S20. Pore-size distributions of CS-Ru-40. An average pore size of 0.55 nm was detected.
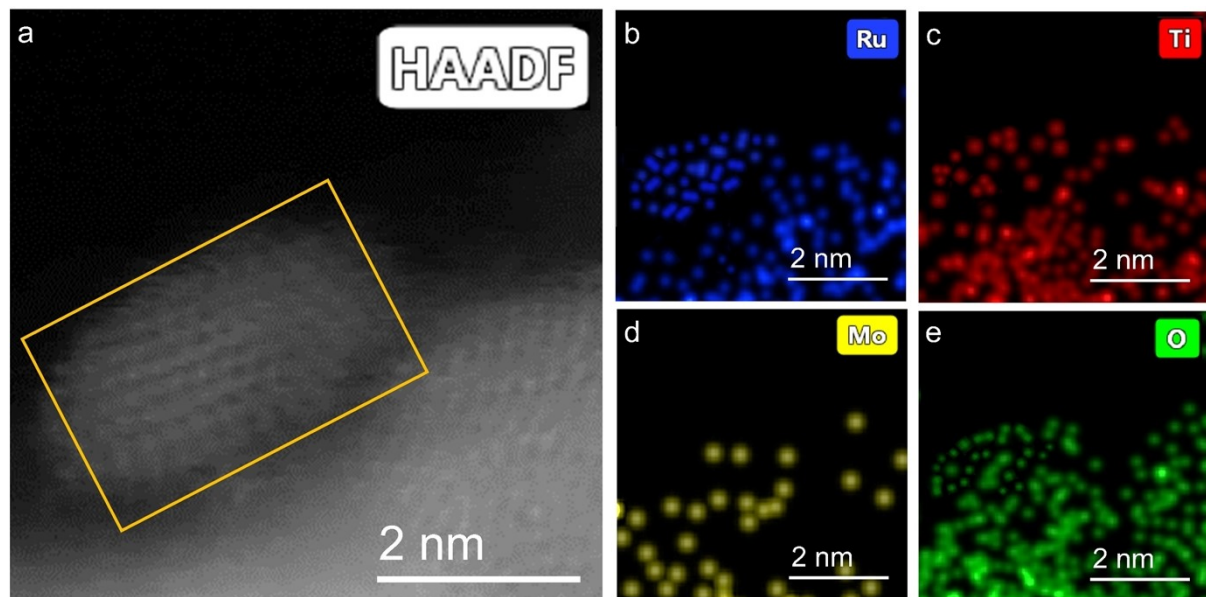
Figure S21. Elemental mapping images of CS-Ru-40 obtained through HAADF-STEM EDS analysis.

DFT calculation computational details

All theoretical calculations were carried out by applying the framework of DFT method with the open-source plane wave set QUANTUM ESPRESSO code[1]. The Standard solid-state pseudopotentials (SSSP) were used to describe ionic cores[2,3]. The cutoff energy of 60 Ry was adopted. The self-consistent-field (SCF) was set to be 10^{-5} eV, and that for geometry optimizations by Broyden-Fletcher-Goldfarb-Shanno (BFGS) algorithm was set to be 0.01 eV Å^{-1} on maximum force component. The k-point sampling of the Brillouin zone was obtained using a 4×2×1 grid for unit by Monkhorst-Pack scheme. Denser k-points (8×4×2) were used for the electronic structure calculations. A large vacuum slab of 15 Å was inserted in z direction for surface isolation to prevent interaction between two neighboring surfaces. Spin polarization was considered in all calculations. The surfaces are constructed based on the optimized bulk structure. After the test, a slab including four atomic layers are chosen to model the Ru (100) @ TiO$_2$ (110) core-shell structure surface. And the model of Mo:Ru/porous TiO$_x$ was constructed by replacing one Ru atom with Mo, and partially removing Ti/O atoms. The bottom two layers are kept frozen to the bulk positions, and the other atoms were relaxed. Further free geometry optimizations and energy calculations were calculated based on the above models. The Bader charges were calculated using the Henkelman algorithm. The energy barrier calculation was performed by the projected velocity Verlet scheme. The free energy of the adsorbed state was calculated as follows based on the adsorption energy (3):

$$\Delta G = \Delta E + \Delta E_{ZPE} - T\Delta S \quad (3)$$

where, ΔE is the adsorption energy of intermediates and ΔE_{ZPE} is the difference corresponding to the zero-point energy between the adsorbed state and the gas phase. The data was obtained from previous research[4,5].
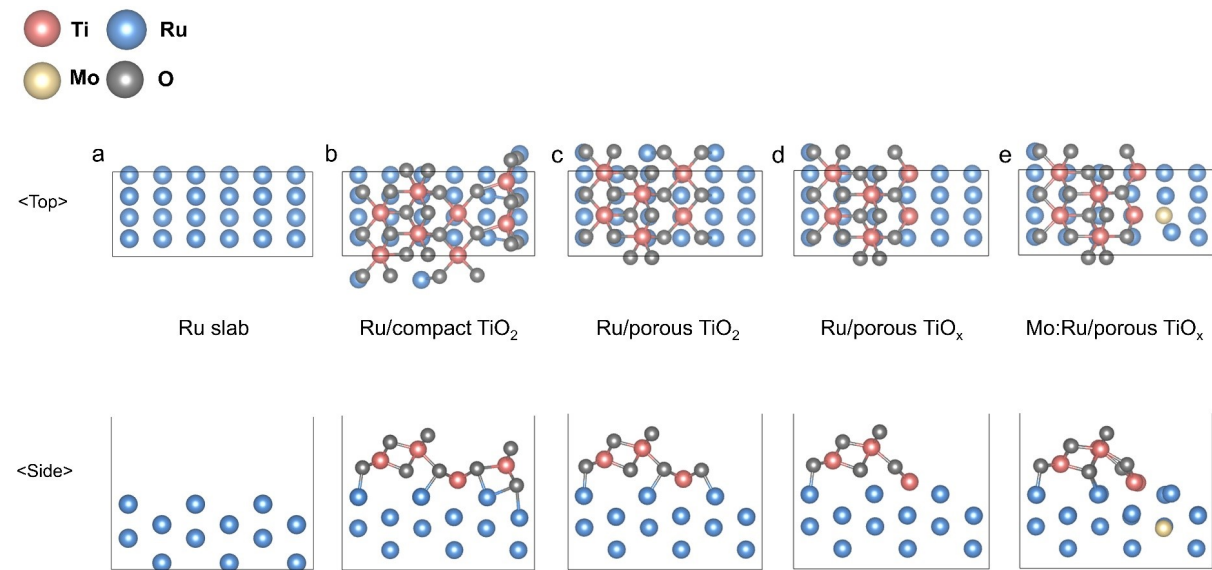
Figure S22. Atomic structure of (a) Ru metal surface, (b) Ru/compact TiO_2, (c) Ru/porous TiO_2, (d) Ru/porous TiO_x, and (e) Mo:Ru/porous TiO_x. Red: titanium atom. Blue: ruthenium atom. Grey: oxygen atom. Yellow: molybdenum atom.
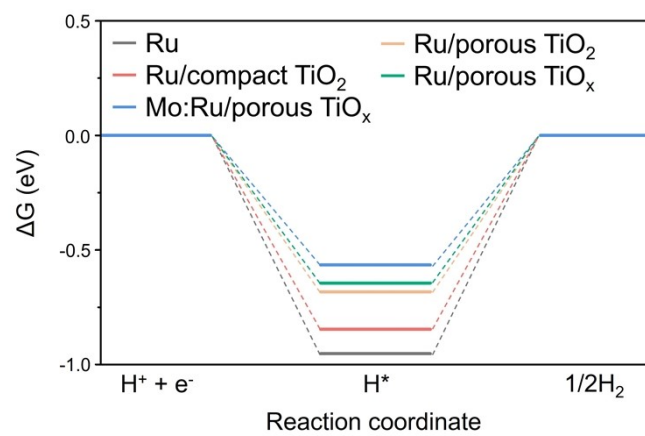
Figure S23. Calculated free energy diagram of hydrogen desorption on pristine Ru, Ru/compact TiO$_2$, Ru/porous TiO$_2$ or TiO$_x$, and Mo:Ru/porous TiO$_x$ surfaces.
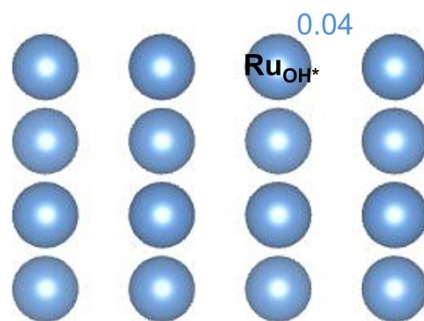
Figure S24. The calculated Bader charge of Ru atoms in the Ru slab, where Ru_{OH*} denotes the atoms to which OH* intermediates are attached following water dissociation.
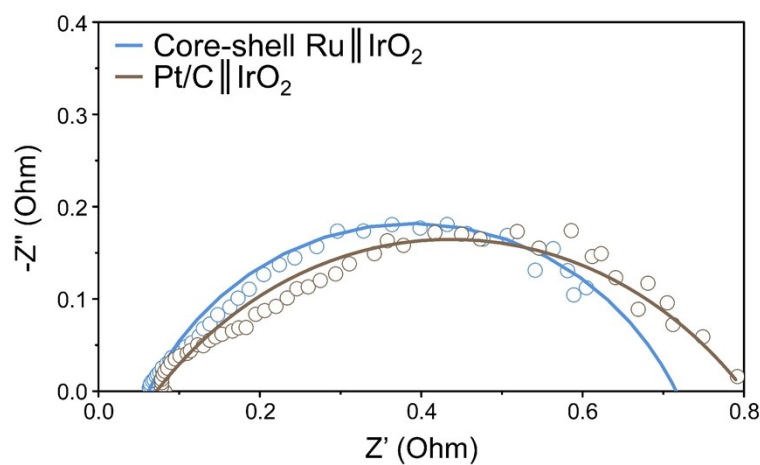
Figure S25. Nyquist plots of the fitting results for the core–shell Ru‖IrO$_2$ and Pt/C‖IrO$_2$. EIS analysis was performed at the current density of 0.1 A cm^{-2} in 1.0 M KOH (pH = 14). Core–shell Ru in this figure corresponds to the catalyst annealed for 40 min (i.e. CS-Ru-40).
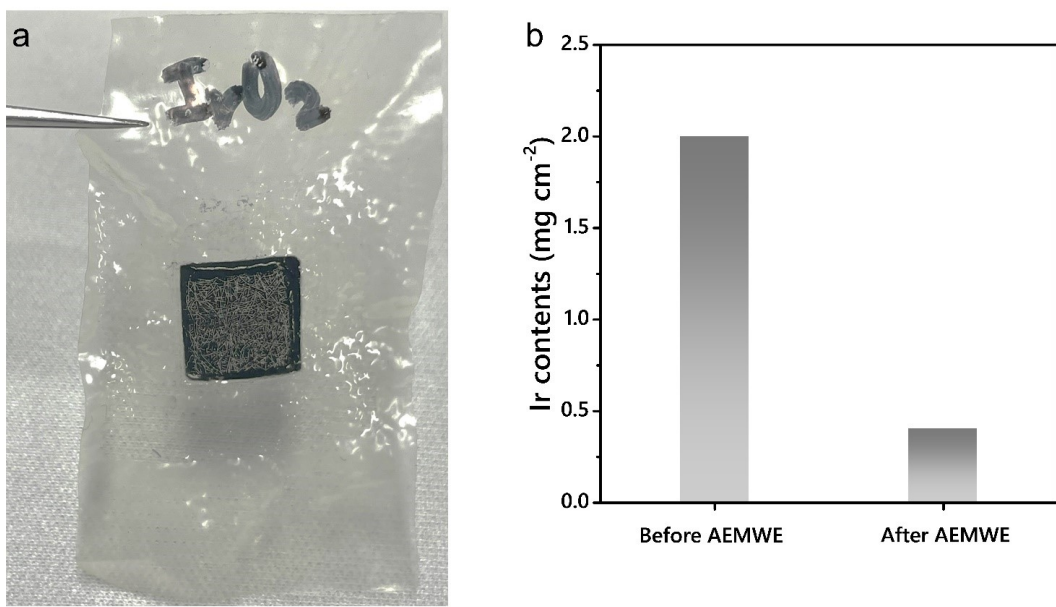
Figure S26. (a) Image and (b) ICP-MS result of IrO_2 electrode after AEMWE measurement.
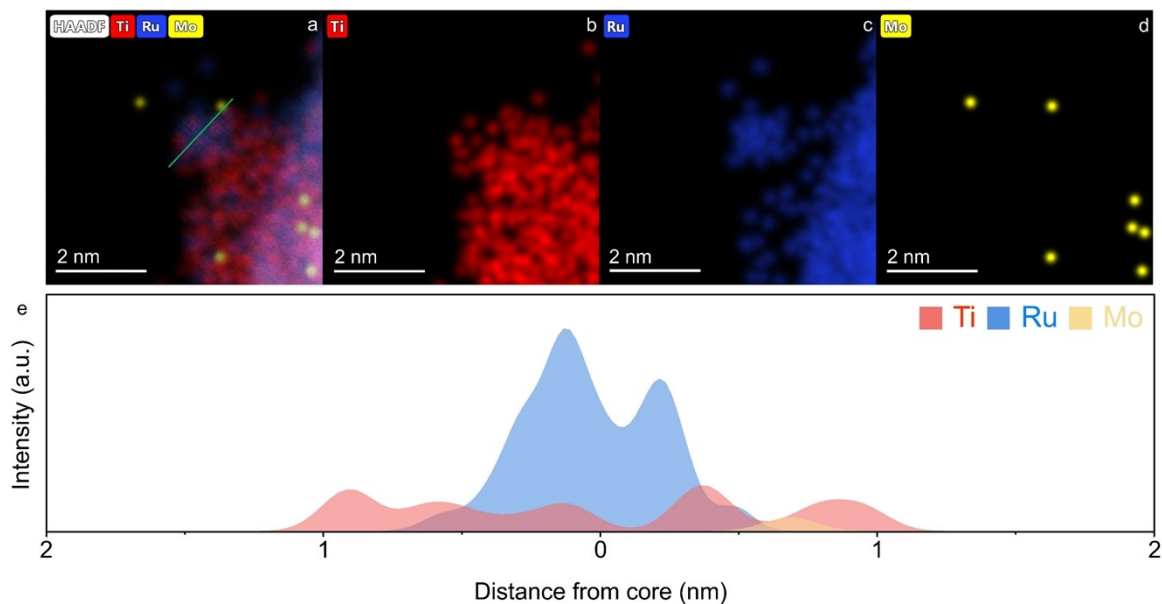
Figure S27. (a) – (d) Elemental mapping images and (e) line-scan profile of CS-Ru-40 NC after AEMWE durability test.

Supplementary Tables

Table S1. Elemental composition and shell thickness of core–shell Ru NCs as a function of annealing time.

	CS-Ru-0	CS-Ru-20	CS-Ru-40	CS-Ru-60
Ti (at%)	4.1	12.3	38.1	45.9
Ru (at%)	94.6	84.3	54.5	44.3
Mo (at%)	1.3	3.4	7.4	9.8
Shell thickness (nm)	0	0	0.45	1.38

Table S2. The proportion of elements of the core–shell Ru, Ru/C, and RuO$_2$/C obtained using ICP-MS analysis.

Core–shell Ru in this table corresponds to the catalyst annealed for 40 min (i.e. CS-Ru-40).

ppb	Core–shell Ru	Ru/C	RuO$_2$/C
Titanium	255813.2	-	-
Ruthenium	158.3	201.3	198.5
Molybdenum	329.1	-	-

Table S3. Comparison of HER performances for core–shell Ru with other HER electrocatalyst. Core–shell Ru in this table corresponds to the catalyst annealed for 40 min (i.e. CS-Ru-40).

Catalysts	Overpotential (mV)	Electrolyte	Reference
Ru@CN	32 (@ 10 mA cm^{-2}) 129 (@50 mA cm^{-2})	1.0 M KOH	6
Ni(OH)$_2$@Ni-N/Ni-C	60 (@ 10 mA cm^{-2}) 112 (@ 50 mA cm^{-2}) 141 (@ 100 mA cm^{-2})	1.0 M KOH	7
Au@Ru	67 (@ 10 mA cm^{-2}) 182 (@ 50 mA cm^{-2})	1.0 M KOH	8
2DPC-RuMo	18 (@ 10 mA cm^{-2}) 53 (@ 50 mA cm^{-2}) 91 (@ 100 mA cm^{-2})	1.0 M KOH	9
RuCo@NC	28 (@ 10 mA cm^{-2})	1.0 M KOH	10
W/WO$_2$	34 (@ 10 mA cm^{-2}) 112 (@ 50 mA cm^{-2}) 202 (@ 100 mA cm^{-2})	1.0 M KOH	11
Ru-NiPS$_3$ NSs	58 (@ 10 mA cm^{-2}) 106 (@ 50 mA cm^{-2}) 129 (@ 100 mA cm^{-2})	1.0 M KOH	12
MoN-5% Os	21.2 (@ 10 mA cm^{-2}) 88 (@ 50 mA cm^{-2}) 133 (@ 100 mA cm^{-2})	1.0 M KOH	13
Pt/C	42 (@ 10 mA cm^{-2}) 133	1.0 M KOH	13

	(@ 50 mA cm^{-2})		
MoS$_2$/NiCo-LDH	78 (@ 10 mA cm^{-2}) 136 (@ 50 mA cm^{-2}) 166 (@ 100 mA cm^{-2})	1.0 M KOH	14
Pd$_3$Ru	42 (@ 10 mA cm^{-2}) 111 (@ 50 mA cm^{-2})	1.0 M KOH	15
Mo-Ru NSA	16 (@ 10 mA cm^{-2}) 39 (@ 50 mA cm^{-2})	1.0 M KOH	16
Pt$_{28}$Mo$_6$Pd$_{28}$Rh$_{27}$Ni$_{15}$	9.7 (@ 10 mA cm^{-2}) 35 (@ 50 mA cm^{-2}) 56 (@ 100 mA cm^{-2})	1.0 M KOH	17
Ni$_3$N/Ni	89 (@ 10 mA cm^{-2}) 210 (@ 50 mA cm^{-2})	1.0 M KOH	18
Ni$_2$P/NiTe$_2$	62 (@ 10 mA cm^{-2}) 119 (@ 50 mA cm^{-2}) 143 (@ 100 mA cm^{-2})	1.0 M KOH	19
V-SRCO	58 (@ 10 mA cm^{-2}) 102 (@ 50 mA cm^{-2}) 142 (@ 100 mA cm^{-2})	1.0 M KOH	20
Pt-Ni	57 (@ 10 mA cm^{-2}) 217 (@ 100 mA cm^{-2})	1.0 M KOH	21
Core–shell Ru	2 (@ 10 mA cm^{-2}) 34 (@ 50 mA cm^{-2}) 51 (@ 100 mA cm^{-2})	1.0 M KOH	**This work**

Table S4. Comparison of activities of MEAs constructed using CCS method. Core–shell Ru in this table

corresponds to the catalyst annealed for 40 min (i.e. CS-Ru-40).

Anode	Cathode	Conditions (Electrolyte / temperature)	Membrane	Activity	Reference
RuO_2	$Pt-MoAl_{1-x}B$	1.0 M KOH 60 °C	X37-50, Grade T, Dioxide Materials	1 A cm^{-2} @ 2.0 V	22
Fe-NiMo-NH$_3$/H$_2$	NiMo-NH$_3$/H$_2$	1.0 M KOH 80 °C	X37-50, Grade T, Dioxide Materials	1 A cm^{-2} @ 1.57 V	23
NiFe-BTC-GNPs	$MoNi_4/MoO_2$	0.1 M KOH 70 °C	FAA-3-PK-130, FumaTech	1.15 A cm^{-2} @ 1.85 V	24
NA-Ru$_3$Ni/C	NA-Ru$_3$Ni/C	1.0 M KOH 60 °C	X37-50, Grade T, Dioxide Materials	1 A cm^{-2} @ 2.048 V	25
Ni foam	Ni@NCW	1.0 M KOH RT	-	0.8 A cm^{-2} @ 1.99 V	26
IrO_2	Ru$_2$P NF	1.0 M KOH 50 °C	X37-50, Dioxide Materials	1.03 A cm^{-2} @ 1.8 V	27
RuO_2	Ru-Ru$_2$P/V$_2$CT$_x$	1.0 M KOH 60 °C	X37-50, Grade T, Dioxide Materials	1 A cm^{-2} @ 1.8 V	28
IrO_2	NS-Ru@NiOH/Ni$_5$P$_4$	1.0 M KOH 50 °C	FAA-3-PK-130, FumaTech	1.5 A cm^{-2} @ 1.8 V	29
Ru-Ni$_2$P/Ni$_5$P$_4$	Ru-Ni$_2$P/Ni$_5$P$_4$	1.0 M KOH 60 °C	-	0.98 A cm^{-2} @ 1.8 V	30
IrO_2	NiRu/C	1.0 M KOH 70 °C	AF-HNN-50-X, Ionomr Innovations	1.2 A cm^{-2} @ 1.8 V	31
RuO_2	α-Co(OH)$_2$@Ru	1.0 M KOH RT	Homemade	0.17 A cm^{-2} @ 1.8 V	32
IrO_2	**Core–shell Ru**	1.0 M KOH 60 °C	PiperION	3.35 A cm^{-2} @ 2.0 V	**This work**

Reference

1 P. Giannozzi, S. Baroni, N. Bonini, M. Calandra, R. Car, C. Cavazzoni, D. Ceresoli, G. L. Chiarotti, M. Cococcioni, I. Dabo, A. Dal Corso, S. De Gironcoli, S. Fabris, G. Fratesi, R. Gebauer, U. Gerstmann, C. Gougoussis, A. Kokalj, M. Lazzeri, L. Martin-Samos, N. Marzari, F. Mauri, R. Mazzarello, S. Paolini, A. Pasquarello, L. Paulatto, C. Sbraccia, S. Scandolo, G. Sclauzero, A. P. Seitsonen, A. Smogunov, P. Umari and R. M. Wentzcovitch, *J. Phys. Condens. Matter*, 2009, **21**, 395502.

2 J. M. Smith, S. P. Jones and L. D. White, *Phys. Rev. B*, 1990, **41**, 7892–7895.

3 K. Lejaeghere, G. Bihlmayer, T. Björkman, P. Blaha, S. Blügel, V. Blum, D. Caliste, I. E. Castelli, S. J. Clark, A. Dal Corso, S. De Gironcoli, T. Deutsch, J. K. Dewhurst, I. Di Marco, C. Draxl, M. Dułak, O. Eriksson, J. A. Flores-Livas, K. F. Garrity, L. Genovese, P. Giannozzi, M. Giantomassi, S. Goedecker, X. Gonze, O. Grånäs, E. K. U. Gross, A. Gulans, F. Gygi, D. R. Hamann, P. J. Hasnip, N. A. W. Holzwarth, D. Iuşan, D. B. Jochym, F. Jollet, D. Jones, G. Kresse, K. Koepernik, E. Küçükbenli, Y. O. Kvashnin, I. L. M. Locht, S. Lubeck, M. Marsman, N. Marzari, U. Nitzsche, L. Nordström, T. Ozaki, L. Paulatto, C. J. Pickard, W. Poelmans, M. I. J. Probert, K. Refson, M. Richter, G. M. Rignanese, S. Saha, M. Scheffler, M. Schlipf, K. Schwarz, S. Sharma, F. Tavazza, P. Thunström, A. Tkatchenko, M. Torrent, D. Vanderbilt, M. J. Van Setten, V. Van Speybroeck, J. M. Wills, J. R. Yates, G. X. Zhang and S. Cottenier, *Science,* 2016, **351**, aad3000.

4 J. K. Nørskov, J. Rossmeisl, A. Logadottir, L. Lindqvist, J. R. Kitchin, T. Bligaard and H. Jónsson, *J. Phys. Chem. B*, 2004, **108**, 17886–17892.

5 J. K. Nørskov, T. Bligaard, A. Logadottir, J. R. Kitchin, J. G. Chen, S. Pandelov and U. Stimming, *J. Electrochem. Soc.*, 2005, **152**, J23.

6 J. Wang, Z. Wei, S. Mao, H. Li and Y. Wang, *Energy Environ. Sci.*, 2018, **11**, 800–806.

7 K. Dastafkan, X. Shen, R. K. Hocking, Q. Meyer and C. Zhao, *Nat. Commun.*, 2023, **14**, 1–10.

8 X. Chen, X. T. Wang, J. B. Le, S. M. Li, X. Wang, Y. J. Zhang, P. Radjenovic, Y. Zhao, Y. H. Wang, X. M. Lin, J. C. Dong and J. F. Li, *Nat. Commun*, 2023, **14**, 5289.

9 K. Tu, D. Tranca, F. Rodríguez-Hernández, K. Jiang, S. Huang, Q. Zheng, M. X. Chen, C. Lu, Y. Su, Z. Chen, H. Mao, C. Yang, J. Jiang, H. W. Liang and X. Zhuang, *Adv. Mater.*, 2020, **32**, 1–10.

10 J. Su, Y. Yang, G. Xia, J. Chen, P. Jiang and Q. Chen, *Nat. Commun*, 2017, **8**, 1–10.

11 Z. Chen, W. Gong, J. Wang, S. Hou, G. Yang, C. Zhu, X. Fan, Y. Li, R. Gao and Y. Cui, *Nat. Commun*, 2023, **14**, 5363.

12 Q. Fu, L. W. Wong, F. Zheng, X. Zheng, C. S. Tsang, K. H. Lai, W. Shen, T. H. Ly, Q. Deng and J. Zhao, *Nat. Commun*, 2023, **14**, 1–11.

13   V. H. Do, P. Prabhu, Y. Li, W. Xie, P. Kidkhunthod, G. Wang, X. Wang and J. M. Lee, *Joule*, 2023, **7**, 2118–2134.

14   J. Hu, C. Zhang, L. Jiang, H. Lin, Y. An, D. Zhou, M. K. H. Leung and S. Yang, *Joule*, 2017, **1**, 383–393.

15   X. Qin, L. Zhang, G. L. Xu, S. Zhu, Q. Wang, M. Gu, X. Zhang, C. Sun, P. B. Balbuena, K. Amine and M. Shao, *ACS Catal.*, 2019, **9**, 9614–9621.

16   L. Li, S. Liu, C. Zhan, Y. Wen, Z. Sun, J. Han, T. S. Chan, Q. Zhang, Z. Hu and X. Huang, *Energy Environ. Sci.*, 2022, **16**, 157–166.

17   M. Wei, Y. Sun, J. Zhang, F. Ai, S. Xi and J. Wang, *Energy Environ. Sci.*, 2023, **16**, 4009–4019.

18   D. Zhang, H. Li, A. Riaz, A. Sharma, W. Liang, Y. Wang, H. Chen, K. Vora, D. Yan, Z. Su, A. Tricoli, C. Zhao, F. J. Beck, K. Reuter, K. Catchpole and S. Karuturi, *Energy Environ. Sci.*, 2022, **15**, 185–195.

19   Y. Li, X. Tan, H. Tan, H. Ren, S. Chen, W. Yang, S. C. Smith and C. Zhao, *Energy Environ. Sci.*, 2020, **13**, 1799–1807.

20   S. Pan, X. Yang, J. Sun, X. Wang, J. Zhu and Y. Fu, *Adv. Energy Mater.*, 2023, **13**, 1–9.

21   J. Kim, S. M. Jung, N. Lee, K. S. Kim, Y. T. Kim and J. K. Kim, *Adv. Mater.*, 2023, **2305844**, 1–10.

22   S. J. Park, T. H. Nguyen, D. T. Tran, V. A. Dinh, J. H. Lee and N. H. Kim, *Energy Environ. Sci.*, 2023, **16**, 4093–4104.

23   P. Chen and X. Hu, *Adv. Energy Mater.*, 2020, **10**, 1–6.

24   P. Thangavel, M. Ha, S. Kumaraguru, A. Meena, A. N. Singh, A. M. Harzandi and K. S. Kim, *Energy Environ. Sci.*, 2020, **13**, 3447–3458.

25   L. Gao, F. Bao, X. Tan, M. Li, Z. Shen, X. Chen, Z. Tang, W. Lai, Y. Lu, P. Huang, C. Ma, S. C. Smith, Z. Ye, Z. Hu and H. Huang, *Energy Environ. Sci.*, 2022, **16**, 285–294.

26   D. Li, H. Cheng, X. Hao, G. Yu, C. Qiu, Y. Xiao, H. Huang, Y. Lu and B. Zhang, *Adv. Mater.*, 2024, **36**, 1–10.

27   J. C. Kim, J. Kim, J. C. Park, S. H. Ahn and D. W. Kim, *Chem. Eng. J.*, 2021, **420**, 130491.

28   T. H. Nguyen, P. K. L. Tran, D. T. Tran, V. A. Dinh, N. H. Kim and J. H. Lee, *Appl. Catal. B-Environ.*, 2024, **343**, 123517.

29   K. Wang, J. Cao, X. Yang, X. Sang, S. Yao, R. Xiang, B. Yang, Z. Li, T. O'Carroll, Q. Zhang, L. Lei, G. Wu and Y. Hou, *Adv. Funct. Mater.*, 2023, **33**, 1–10.

30   Y. Xia, L. Guo, J. Zhu, J. Tang, Z. Li, X. Liu, J. Chi and L. Wang, *Appl. Catal. B-Environ.*, 2024, **351**, 123995.

31   S. Ruck, A. Körner, A. Hutzler, M. Bierling, J. Gonzalez, W. Qu, C. Bock, S. Thiele, R. Peach and C. V. Pham,

JPhys Energy, 2022, **4**, 044007.

32   J. Zhao, J. Wang, X. Zheng, H. Wang, J. Zhang, J. Ding, X. Han, Y. Deng and W. Hu, *Small Methods*, 2023, **7**,

1–9.